Aircraft Wake Evolution Prediction Based on Parallel Hybrid Neural Network Model

Leilei Deng , Weijun Pan * , Yuhao Wang , Tian Luan , Yuanfei Leng

Posted Date: 13 May 2024

doi: 10.20944/preprints202405.0814.v1

Keywords: CFD; prediction of aircraft wake evolution; parallel architecture; intelligent aerodynamics; approach phase

Article

Aircraft Wake Evolution Prediction Based on Parallel Hybrid Neural Network Model

Leilei Deng [1], Weijun Pan [1,*], Yuhao Wang, [1] Tian Luan [1] and Yuanfei Leng [2]

[1] School of Air Traffic Management, Civil Aviation Flight University of China, Guanghan 618307, China; deng_leilei@cafuc.edu.cn(L.D.); guiltybutcher@163.com(Y.W.); dp_nnsm22@163.com(T.L.)
[2] School of Electronic and Information Engineering, Beihang University, Beijing 100000, China; BY2302108@buaa.edu.cn
* Correspondence: wjpan@cafuc.edu.cn(W.P.)

Abstract: To overcome the time-consuming drawbacks of Computational Fluid Dynamics (CFD) numerical simulations, this paper proposes a hybrid model based on a parallel architecture based on the concept of intelligent aerodynamics, named PA-TLA (Parallel Architecture combining TCN, LSTM, and Attention mechanism). This model utilizes CFD data to drive efficient predictions of aircraft wake evolution at different initial altitudes during the approach phase. Initially, CFD simulations of continuous initial altitudes during the approach phase are used to generate aircraft wake evolution data, which are then validated against real-world LIDAR data to verify their reliability. The PA-TLA model is designed based on a parallel architecture, combining Long Short-Term Memory networks (LSTM), Temporal Convolutional Networks (TCN), and a tensor concatenation module based on the attention mechanism, which ensures computational efficiency while fully leveraging the advantages of each component in a parallel processing framework. The study results show that the PA-TLA model outperforms both the LSTM and TCN models in predicting the three characteristic parameters of aircraft wake: vorticity, circulation, and Q-criterion. Compared to the serially structured TCN-LSTM, PA-TLA achieves an average reduction in mean squared error (MSE) by 6.80%, mean absolute error (MAE) by 7.70%, and root mean square error (RMSE) by 4.47%, with an average increase in the coefficient of determination (R^2) by 0.36%, and a 35% improvement in prediction efficiency. Lastly, this study combines numerical simulation and the PA-TLA deep learning architecture to analyze the characteristics of wake evolution during the near-ground phase, providing theoretical value for further reducing aircraft wake intervals and enhancing airport operational efficiency.

Keywords: CFD; prediction of aircraft wake evolution; parallel architecture; intelligent aerodynamics; approach phase;

1. Introduction

Aircraft wake turbulence is a byproduct of lift generation, characterized by its long duration, wide distribution, and high intensity. When an aircraft enters the wake region of a leading aircraft, the intense vortical structures induce rolling torques, causing the trailing aircraft to experience bumps, rolls, and changes in flight status. According to the Federal Aviation Administration (FAA), 78% of wake encounters occurred below 200 feet (61 meters) from 1983 to 2000 [13]. During the approach phase, aircraft density increases along the glide path and, influenced by ground effect, the wake may stall or rebound near the ground [14], hence the evolution of wake vortices varies at different heights during this phase. Wake separation also limits the number of flights that can take off and land at an airport per unit of time, significantly impacting airport capacity.

In the early 1970s, the International Civil Aviation Organization (ICAO) established standards for aircraft wake separation, which proved overly conservative due to a lack of consideration for meteorological factors and specific scenarios. To establish reasonable standards for the spacing of aircraft during approach and departure, and to effectively enhance airport capacity and air traffic operational efficiency, numerous scholars have begun systematic studies on aircraft wake, exploring its physical mechanisms. Traditional wake monitoring and prediction technologies include Computational Fluid Dynamics (CFD) simulations, wind tunnel and water tunnel experiments, and

 doi:10.20944/preprints202405.0814.v1

field radar detection. CFD simulations, in particular, simulate the characteristics and evolution of aircraft wake near the ground across various environments. Under clear sky conditions, classical numerical simulation techniques primarily involve Large Eddy Simulation (LES) methods and Reynolds-Averaged Navier-Stokes approaches. Holzäpfel and others [15, 16] used aircraft wake velocity models as initial conditions for numerical simulations, significantly enhancing computational efficiency and accuracy. In terms of wake velocity models, research institutions in Europe and America, including the German Aerospace Center (DLR), the French company Thales, and the National Aeronautics and Space Administration (NASA), have combined theoretical analysis, numerical simulation, and extensive experimental measurements to obtain the tangential velocity distribution of aircraft wake on cross-sections [17], with representative models including Lamb-Oseen, Hallock-Burnham, Proctor, and Winckelmans.

During the approach phase, the initial altitude of wake evolution varies, and wake vortices can be classified as either Out of Ground Effect (OGE) or In Ground Effect (IGE). Crow first analyzed the linear stability of vortex pairs in the OGE region [18]. He discovered that under certain disturbances, vortex pairs would incline about 45 degrees into a symmetric fixed plane and form sinusoidal shapes. Subsequently, the vortex pairs connect at their closest points, leading to the formation of a helical structure and the destruction of wake vortices, known as long-wave instability or Crow instability. Holzapfel et al. and Han et al. used LES and Direct Numerical Simulation (DNS) to analyze the evolution of OGE vortices, concluding that background atmospheric turbulence dictates the long-wave instability [19-21], such as wake vortex stretching and the generation of Secondary Vortex Structures (SVS) in weak to moderate background turbulence. Meanwhile, these SVS consume primary vortex energy, ultimately leading to extensive deformation. In strong background turbulence, the intensity of primary vortices is insufficient to affect atmospheric vortices; IGE wake vortices affected by ground effects occur below 1.5b0 (b0, initial vortex pair separation) [22]. Harvey and others first introduced secondary vortices generated by boundary layer separation; their upward-induced velocity caused the primary vortex to rebound [23]. Additionally, image vortices near the ground increase the separation between primary vortices, making it difficult to trigger horizontal long-wave instability. These factors lead to longer hovering times of wake over runways, increasing encounter risks. Harris and Williamson conducted experimental studies on IGE wake vortex evolution [24], showing that at lower Reynolds numbers, SVS overall bends, exhibiting Crow-type instability. However, few studies have fully examined the continuous initial altitude evolution of OGE and IGE wake vortices during the approach phase.

In recent years, with the rapid development of artificial intelligence, the close integration of aerodynamics and intelligent technologies has given rise to a new interdisciplinary field—intelligent aerodynamics. This field incorporates the unique research methods of the fourth research paradigm (data-driven), combining AI's rapid and precise predictive capabilities with the large data computation models of aerodynamics, making it possible to deduce complex scenario evolution outcomes from calculations of typical scenarios alone. Compared to experimental and computational aerodynamics, intelligent aerodynamics primarily features the comprehensive application of multiple research methods and data, significantly enhancing efficiency, accuracy, and applicability. It also bridges "technology gaps" such as unclear mechanisms and insufficient computing power through "end-to-end" modeling, addressing aerodynamic problems that traditional methods struggle to solve. Zheng Tianyun and others [5] used the SSTγ-Reθ transition model's extensive zero-pressure gradient natural transition flat plate calculations as training data, employing deep residual networks to reconstruct the mapping between local mean values and the intermittency factor γ, developing an efficient AI-based transition model. Wu Lei and others [6] established an artificial neural network mapping from mean flow field information to the transition intermittency factor γ using numerical simulation results of the SST-γ transition model as the training test set, coupling it with the RANS solver to predict the transition locations and simulate transition flow fields for various airfoil profiles, achieving good generalization. Carpenter and others [7] proposed a single-hidden-layer neural network for predicting missile aerodynamic parameters. Balla and others [8] introduced a multi-output neural network for predicting two-dimensional and three-dimensional wing aerodynamic

 doi:10.20944/preprints202405.0814.v1

coefficients, outperforming their inherent Orthogonal Decomposition (POD) method. Wang and others [9] proposed a deep learning-based model, which while achieving more accurate flow field characteristics, significantly reduced computational costs.

By systematically observing and analyzing wake vortex circulation, vortex core radius, diffusion distance, and other wake dissipation characteristics, and based on these, establishing a wake characteristic database for early prediction in wake risk zones, the continuous initial altitude evolution of wake vortices during the approach phase is researched. However, ensuring identical conditions in each practical experiment is challenging, and the resolution of observational equipment such as lidar limits the detailed capture of wake evolution processes. Using numerical simulation as a supplement, while complex in computational process, demanding in resources, and lengthy in time, enables exhaustive computation across all scenarios. Thus, in the rapidly evolving field of intelligent aerodynamics, combining numerical simulation data with deep learning to achieve flow field predictions represents a future development trend. Recurrent Neural Networks (RNN) and Convolutional Neural Networks (CNN) are commonly used deep learning models for processing sequence data. RNNs are particularly suited for tasks with time dependencies but are limited by the gradient vanishing problem in training, making them challenging for long-term dependency tasks. To address this issue, Long Short-Term Memory (LSTM) networks have been introduced. CNNs, by extracting complex features from time series, effectively recognize local feature correlations, and their local connectivity and feature-sharing properties greatly enhance prediction efficiency. Based on CNNs, Temporal Convolutional Networks (TCN) further study time series feature relationships, improving the extraction of cross-time series relationships and prediction efficiency through causal convolution and dilated convolution. Currently, traditional machine learning algorithms are also widely used in flow field predictions. Xu and others, based on an unsteady flow field dataset around a cylinder, involved the CAE-LSTM model in flow field predictions [11]. He and others proposed a CNN-based wake vortex prediction model, predicting aircraft wake vortex evolution under different side wind speeds [12]. Mohan and others used a hybrid neural network combining CNN and LSTM to extract coherent structures of turbulence [1].

Despite this, facing complex and voluminous numerical simulation data, single models are no longer sufficient. However, classical hybrid models, due to their serial architecture, result in long computational times. In light of this, this study proposes the use of CFD simulation data-driven, parallel architecture-based hybrid models—the PA-TCN-LSTM-Attention model (PA-ATL)—combining TCN, LSTM, and attention mechanism modules with tensor connection modules to predict aircraft wake evolution during the approach phase, comprehensively mastering the continuous initial altitude wake dissipation mechanisms. In this model, TCN and LSTM operate independently, but their shared goal is to capture key features such as long-term dependencies and context information. TCN primarily focuses on local features and long-term dependencies in time series data through multi-stack dilated causal convolution operations; LSTM maintains global awareness of the entire series through gated units, retaining past information in hidden layers to transmit context information; then, based on attention mechanism modules, the tensor connection module dynamically weights the output matrices of both models according to task demands and merges them on the feature dimension to achieve feature fusion. The basic idea of this method is the concept of a parallel architecture, where all individual models in the hybrid model are trained side-by-side independently, learning feature information from the original time series independently before the tensor connection module based on the attention mechanism. This hybrid model's depth is only influenced by the depth of each individual model's network layers.

The main contributions are as follows:

1. Utilizing deep learning neural networks to predict aircraft wake evolution, addressing the long computational times of numerical simulations.
2. Proposing a hybrid deep learning neural network model with a parallel processing structure, extracting feature information from the time series of aircraft wake evolution.
3. Analyzing the characteristics of aircraft near-ground wake evolution, providing theoretical value for enhancing airport operational efficiency.

Preprints.org (www.preprints.org) | NOT PEER-REVIEWED | Posted: 13 May 2024 doi:10.20944/preprints202405.0814.v1

The remainder of this paper is organized as follows: Section 2 introduces the aircraft wake numerical simulation methods employed, feature parameter extraction, and a detailed description of the proposed PA-TLA framework; Section 3 describes how high-fidelity aircraft wake simulation data is generated in CFD, compared with field-detected lidar data, and the PA-TLA model's predictive effectiveness is validated, concluding with an analysis of near-ground wake evolution characteristics combining numerical simulation and the PA-TLA model. Section 4 includes related discussions and summaries.

2. Methodology

Figure 1 presents the flowchart of the prediction framework for aircraft wake evolution during the approach phase. This framework integrates numerical simulation with the proposed parallel hybrid architecture, PA-TLA. The first step involves simulating the aircraft wake at different continuous altitudes during the approach phase and validating these simulations using lidar detection data, as detailed in section 2.1. The second step extracts characteristic parameters of aircraft wake evolution, selecting circulation, vorticity, and the Q-criterion as parameters to quantify the characteristics of wake vortices, as described in section 2.2. The third step employs the Pearson correlation coefficient method to analyze the correlation between altitude and characteristic parameters, as outlined in section 2.3. The fourth step involves constructing the PA-TLA model based on a parallel hybrid architecture to predict aircraft wake characteristic parameters, with the detailed construction process provided in section 2.4.

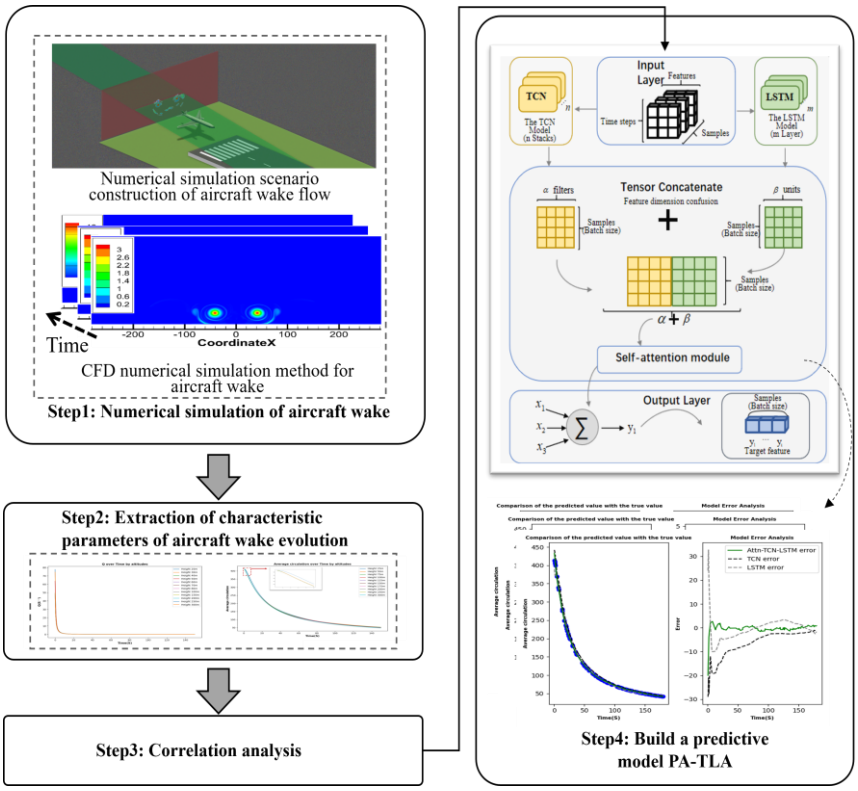

Figure 1. PA-TCN-LSTM-Attention Model Flowchart.

2.1. Aircraft Wake Vortex Numerical Simulation

2.1.1. Aircraft Wake Vortex Numerical Simulation Scenario Construction

Aircraft wake turbulence, an inevitable byproduct of lift generation during flight, includes tip vortices, boundary layer turbulence, and engine jet wash. As the aircraft flies, the pressure increases below the wing while it decreases above, causing the airflow beneath the wing to curl around the wingtip towards the lower-pressure surface above, thus forming high-speed spiral airflows centered around the wingtips behind the aircraft. The two wingtips correspond to two counter-rotating

 doi:10.20944/preprints202405.0814.v1

vortices, with the left wingtip vortex rotating clockwise and the right wingtip vortex rotating counterclockwise, known as tip vortices. The lifecycle of boundary layer turbulence and engine jet wash is short with a limited action distance, posing little harm to subsequent aircraft. In contrast, tip vortices are characterized by long duration, wide distribution, and high intensity, significantly impacting the flight safety of following aircraft. This is the focus of the study. Figure 2 illustrates the generation of aircraft wake vortices [25].

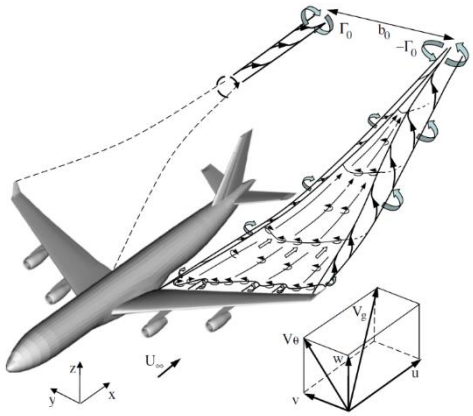

Figure 2. Schematic Diagram of Aircraft Wake Vortex Formation.

Given that the A330 aircraft has the highest flight frequency at Chinese airports, making it one of the most common heavy aircraft types, this paper selects the A330-200 as the object of study. Since the horizontal tail vortices rapidly merge with the wingtip vortices and have a lesser impact on the safety of following aircraft [26], to save computational resources, only the wing part is retained in the simulation examples. Additionally, to simulate and model the evolution process of the wingtip vortices, the winglet part of the wing tip is also retained. The wing model is illustrated in Figure 3.

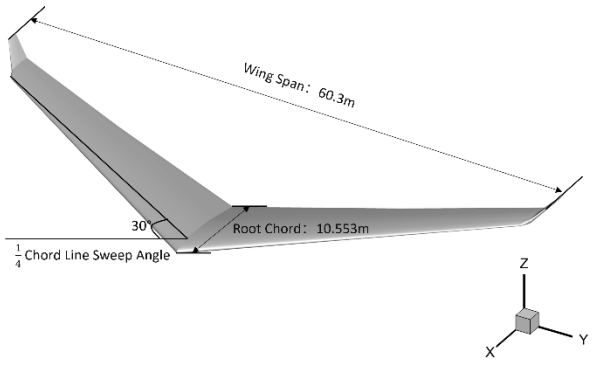

Figure 3. A330-200 Aircraft Wing Model.

The final approach refers to the flight segment in which an aircraft descends along the landing trajectory and aligns with the runway for landing . Generally, it begins from the final approach fix, where the aircraft maintains its final approach trajectory in alignment with the runway centerline extension, and starts the approach with a 5.2% descent gradient, equivalent to a 3° glide slope. Due to the relatively stable flight speed, trajectory, and high overlap within this segment, many scholars have chosen the aircraft wake during the final approach phase as the primary research subject. However, current research often considers only the ground effect at a single altitude, lacking

Preprints.org (www.preprints.org) | NOT PEER-REVIEWED | Posted: 13 May 2024 doi:10.20944/preprints202405.0814.v1

observational experiments on the impact of ground effects at different altitudes. This makes it challenging to determine at which altitude the ground effect on aircraft wake poses the greatest threat to following aircraft.

In view of this, starting from the perspective of studying the wake dissipation mechanism influenced by continuous different approach altitudes, this paper utilizes the User-Defined Function (UDF) secondary development interface tool attached to the FLUENT software. It selects the Hallock-Burnham tangential velocity model for the initial model of the wake vortex, structures the flow domain into grids, and sets the global grid resolution to 0.5m≈0.021b_0, that is, the grid size is 0.5*0.5m. The calculation domain, where the x-direction is the aircraft's approach direction, y-direction is the wingspan direction, and z-direction is the altitude direction, forms a hexahedral configuration of $5b_0 \times 13b_0 \times (2b_0 + H)$. This is illustrated in Figure 4.

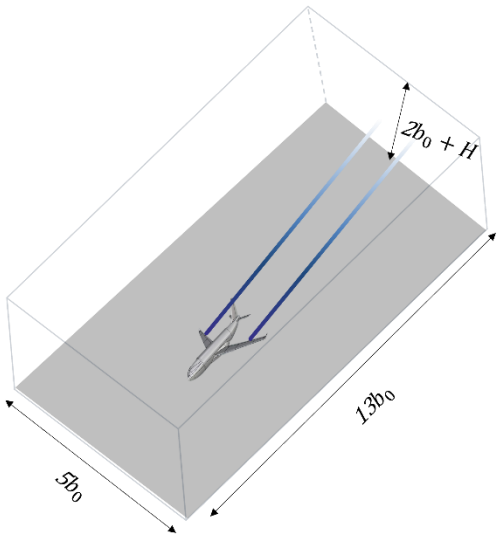

Figure 4. Computational Domain of A330-200.

2.1.2. Wake Vortex Tangential Velocity Model

Tangential velocity is a crucial parameter for describing the characteristics of aircraft wake vortices. By the mid-20th century, numerous scholars proposed models for the tangential velocity profiles of aircraft wake vortices either by solving fluid equations or fitting observational data. Among them, the Lamb-Oseen vortex tangential velocity model, the Hallock-Burnham vortex tangential velocity model, and the Adapted Vortex tangential velocity model are the most widely used. The tangential velocities obtained from these models are generally consistent at distances far from the vortex core. Extensive experiments have confirmed that the Hallock-Burnham velocity model largely agrees with the measured data [27], and the Hallock-Burnham velocity model has a simple and unified velocity expression, making it convenient for theoretical analysis and analytical representation. Therefore, the Hallock-Burnham vortex model is used for simulating the induced velocity of aircraft wake, as Eq.(1):

$$V_T(r) = \frac{\Gamma_0}{2\pi r} \frac{r^2}{r^2 + r_c} \quad (1)$$

Where $V_r(r)$ is the tangential induced velocity at the point; r is the straight-line distance between the point and the core of the vortex; r_0 stands for the vortex core radius; Γ_0 denotes the initial circulation, and r_c is the vortex core radius of the wake vortex.

2.1.3. Aircraft Wake Vortex CFD Numerical Simulation Method

In practical research work, if only the average quantities over time of turbulent motion characteristics are taken as the research object (such as the average velocity field, average forces, etc.),

 doi:10.20944/preprints202405.0814.v1

one can perform an ensemble average on the Navier-Stokes (N-S) equations. By solving the time-averaged N-S equations for turbulence, one can quickly simulate the motion of turbulence. This method of averaging the unsteady N-S equations over time to solve for the time-averaged quantities needed in engineering is known as Reynolds-Averaged Simulation (RAS) [27].

For three-dimensional incompressible fluids, the tensor form of their control equations can be expressed as follows:

$$\frac{\partial \rho}{\partial t}+\frac{\partial\left(\rho \overline{u_i}\right)}{\partial x_i}=0 \tag{2}$$

$$\frac{\partial\left(\rho \overline{u_i}\right)}{\partial t}+\frac{\partial\left(\rho \overline{u_i} \overline{u_j}\right)}{\partial x_j}=-\frac{\partial p}{\partial x_i}+\frac{\partial \sigma_{ij}}{\partial x_j}+\frac{\partial}{\partial x_j}\left(-\rho \overline{u'_i u'_j}\right) \tag{3}$$

where p is the fluid pressure; ρ is the density of atmospheric turbulence; x_i and x_j are Cartesian coordinates; u_i is the mean velocity component in the x_i direction; u_j is the mean velocity component in the x_j direction; u_i' and u_j' are the fluctuating velocity components that contribute to the stress term in the Reynolds-averaged Navier-Stokes equation; represents the components of the stress tensor; and $-\rho \overline{u'_i u'_j}$ denotes the Reynolds stress term.

After ensemble averaging, the resulting Reynolds-averaged equation includes not only the average pressure forces, average molecular viscous forces, and average mass forces but also an additional stress action $-\rho \overline{u'_i u'_j}$, namely the Reynolds stress.

This term is a second-order symmetric tensor, and its expression is as follows:

$$R_{ij}=-\rho\begin{pmatrix}\overline{u'u'} & \overline{u'v'} & \overline{u'w'}\\ \overline{v'u'} & \overline{v'v'} & \overline{v'w'}\\ \overline{w'u'} & \overline{w'u'} & \overline{w'w'}\end{pmatrix} \tag{4}$$

The existence of the Reynolds stress term makes the equations unclosed, necessitating the introduction of turbulence models to simulate the Reynolds stress in the equations, which then allows for the solution of the average flow field.

Current turbulence models mainly include the Reynolds Stress Model (RSM) or eddy-viscosity closure turbulence models, which encompass zero-equation models, one-equation models, and two-equation models, among others [28].

Among these, the Shear-Stress Transport SST $k-\omega$ model offers higher accuracy and reliability compared to the standard SST $k-\omega$ model, especially for rotational flow situations where its advantages are more pronounced. However, due to the SST $k-\omega$ model's strong dependence on wall distance, this model is not suitable for simulating free shear flow.

The transport equations of the SST $k-\omega$ model is expressed as follows:

$$\frac{\partial}{\partial t}(\rho k)+\frac{\partial}{\partial x_i}(\rho k u_i)=\frac{\partial}{\partial x_i}\left[\Gamma_k \frac{\partial k}{\partial x_j}\right]+G_k-Y_k+S_k \tag{5}$$

$$\frac{\partial}{\partial t}(\rho \omega)+\frac{\partial}{\partial x_i}(\rho \omega u_i)=\frac{\partial}{\partial x_j}\left[\Gamma_\omega \frac{\partial \omega}{\partial x_j}\right]+G_\omega-Y_\omega+D_\varepsilon+S_\varepsilon \tag{6}$$

Where G_k represents the turbulent kinetic energy generated by the velocity gradient of the laminar flow; G_ω is derived from the ω (specific rate of dissipation) equation; Γ_k and Γ_ω are the diffusion rates for k (turbulent kinetic energy) and ω respectively; Y_k and Y_ω pertain to the turbulence generated by the diffusion of k and ω; D_ω represents the term for orthogonal

 doi:10.20944/preprints202405.0814.v1

divergence; S_k and S_ω are the source terms for turbulent kinetic energy and turbulence dissipation, respectively, acting as customizable terms.

2.2. Extraction of Aircraft Wake Evolution Characteristic Parameters

To more intuitively and clearly understand the evolution patterns of aircraft wake vortices, parameters such as circulation, vorticity, and the Q criterion are commonly used to quantify wake vortex characteristics.

Circulation is the path integral of fluid velocity (i.e., the tangential velocity of the wake vortex) along a closed curve, typically denoted by Γ. Its expression is as follows:

$$\Gamma = \oint_L \vec{\mathbb{Z}} \bullet ds = \oint_L \mathbb{Z} \cos\alpha ds \quad (7)$$

where Lrepresents the closed curve, and α signifies the angle between the velocity vector and the tangent direction of the point on the line.

According to the Kutta–Joukowsky theorem [1], the circulation of an aircraft's wake is related to various factors such as flight speed and wing shape. When an aircraft with a lift coefficient C_L aspect ratio A_R and wingspan B flies at a speed V ,the lift it generates equals the momentum flux of the rolled-up wake vortices. This can be expressed as

$$\frac{\rho C_L}{2A_R} B^2 V^2 = \rho V b_0 \Gamma_0 \quad (8)$$

$$b_0 = B \bullet s \quad (9)$$

Where b_0 is the initial spacing between the rolled-up vortices; s is the load factor along the wingspan direction (under the assumption of elliptical wings [2], which is approximately true for commercial airliners, and is about $\pi/4$); ρ is the air density.

Thus, the initial circulation Γ_0 of the aircraft's wake can be described as follows:

$$\Gamma_0 = \frac{C_L V B}{2 s A_R} \quad (10)$$

$$\Gamma_0 = \frac{Mg}{\rho s B V} = \frac{4Mg}{\rho \pi B V} \quad (11)$$

where M is the mass of the aircraft.

In numerical simulations, the calculation method for circulation involves taking the average of the area integrals of vorticity on 11 circular planes (centered at the vortex core, with radii ranging from 5 to 15 meters) [3], and then normalizing it with the initial circulation for dimensionless representation, as Eq. (12):

$$\Gamma^*_{5-15} = \frac{1}{11} \sum_{r=5}^{15} \left(\int_0^r \omega dA \right) / \Gamma_0 \quad (12)$$

Vorticity is another crucial parameter characterizing the strength of aircraft wake vortices, with its physical significance being the description of the curl of the velocity vector of the fluid. For a three-dimensional flow field, the vector form of vorticity can be expressed as follows:

$$\overline{\omega} = \nabla \times \overline{V} = \det \begin{vmatrix} \hat{e}_x & \hat{e}_y & \hat{e}_z \\ \frac{\partial}{\partial x} & \frac{\partial}{\partial y} & \frac{\partial}{\partial z} \\ u & v & w \end{vmatrix} = \begin{bmatrix} \partial w/\partial y - \partial v/\partial z \\ \partial u/\partial z - \partial w/\partial x \\ \partial v/\partial x - \partial u/\partial y \end{bmatrix} = \begin{bmatrix} \omega_x \\ \omega_y \\ \omega_z \end{bmatrix} \quad (13)$$

where ω_x, ω_y, ω_z represent the components of vorticity in the x, y and z directions, respectively.

 doi:10.20944/preprints202405.0814.v1

In the case of a two-dimensional planar flow field, since vorticity has components in only one direction, it can be represented by the component of vorticity in the Z direction, as Eq. (14)

$$\omega = \omega_z = \left[\partial v / \partial x - \partial u / \partial y\right] \quad (14)$$

The Q criterion is a physical criterion used to describe the structure and evolution of vortices in fluid flow by calculating the fluid velocity gradient tensor, aiming to quantify the presence and strength of vortices in the flow field using the eigenvalues of this gradient tensor. Unlike traditional velocity vector fields, the Q criterion can intuitively display details such as vortices and boundary layers, and uses the eigenvalues of the gradient tensor to assess the intensity of eddies. The two-dimensional dimensionless Q criterion for the oxz plane can be expressed as:

$$Q = -\frac{1}{2}[(\frac{\partial u}{\partial x})^2 + (\frac{\partial v}{\partial z})^2] - \frac{\partial u}{\partial z}\frac{\partial v}{\partial x} \quad (15)$$

where u and v represent the velocity components in the x and z directions, respectively. When the Q value is greater than 0, the point can be considered as part of a vortex. This approach effectively highlights regions in the flow where the rotation dominates the strain, thus identifying the core areas of vortices.

2.3. Correlation Analysis

To investigate the effect of the initial altitude at which aircraft wake vortices are generated on their evolution, an analysis of the correlation between altitude and extracted wake vortex parameters was conducted using the Pearson correlation coefficient. According to Figure 5, there is a positive correlation coefficient of 0.22 between altitude and the initial circulation of the aircraft wake vortex, indicating that as altitude increases, the initial circulation of the wake vortex also tends to increase. Moreover, the correlation coefficient between altitude and the Q-criterion value of the aircraft wake vortex is -0.77, demonstrating a strong negative correlation. This suggests that as altitude increases, the Q-criterion value of the aircraft wake vortex tends to decrease, indicating that the evolution of aircraft wake is significantly influenced by altitude.

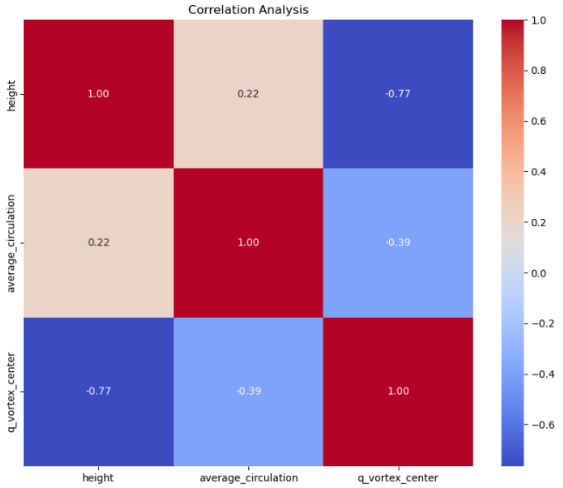

Figure 5. Correlation Coefficient Heatmap.

2.4. Wake Parameter Prediction Model Based on PA-TLA

TCN (Temporal Convolutional Network) and LSTM (Long Short-Term Memory) networks each have their advantages and are suitable for different scenarios. TCN employs a multi-stacked, dilated causal convolution process to focus on the local features of time series data. On the other hand, LSTM uses gated units to maintain a global perception of the entire sequence, storing previous information in hidden layers to transmit contextual information. However, classical serial hybrid framework

Preprints.org (www.preprints.org) | NOT PEER-REVIEWED | Posted: 13 May 2024 doi:10.20944/preprints202405.0814.v1

models increase the demand for computational memory and time, neglecting the increase in the number of model parameters and complexity, leading to higher computational costs during training and reduced timeliness. Therefore, this study proposes a hybrid deep learning model based on a parallel architecture that combines Temporal Convolutional Networks (TCN) and Long Short-Term Memory (LSTM) neural networks through a tensor fusion module based on attention mechanisms for predicting aircraft wake vortex parameters and safety intervals. TCN and LSTM operate independently to capture key features, such as long-term dependencies and contextual information. Finally, through tensor fusion based on the attention mechanism, the output matrices of TCN and LSTM are assigned different attention weights. These are dynamically weighted according to task requirements and merged in the feature dimension to achieve feature information fusion. The depth of the model in this parallel mode is only affected by the depth of each individual network layer. The structure of the model is illustrated in the figure, and this configuration is referred to as the Parallel Architecture LSTM-TCN-Attention (PA-TLA), as shown in Figure 6.

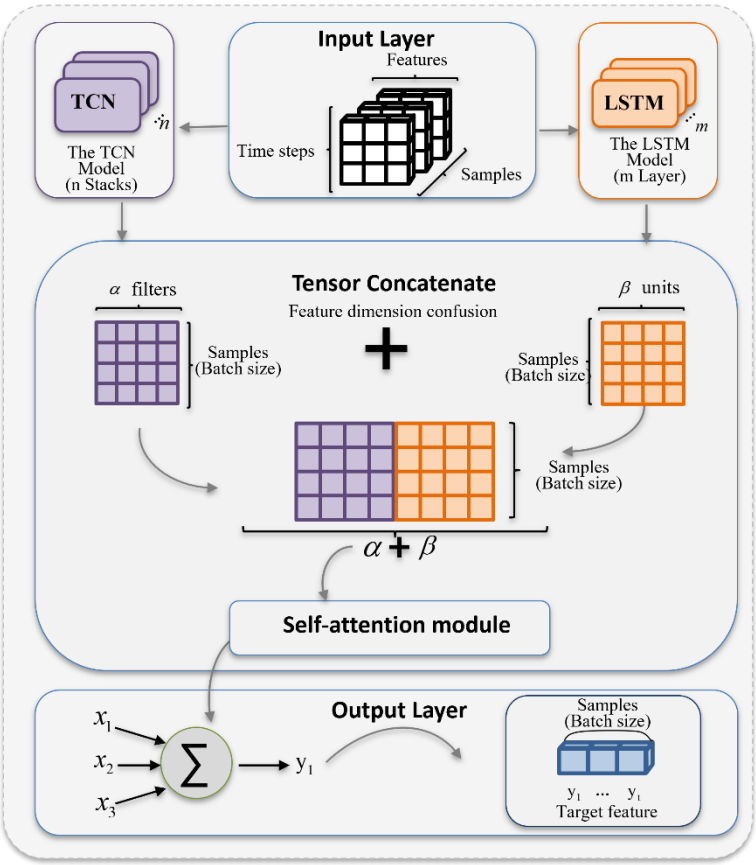

Figure 6. PA-TLA Model Architecture Diagram.

2.4.1. Sequence Space Feature Representation Based on TCN

The Temporal Convolutional Network (TCN) is a model based on the CNN architecture designed for processing time-series data. In this study, we employ the TCN network as a branch of the PA-TLA prediction network to extract global spatial features of sequences. The TCN consists of a stack of multiple residual units. Each residual module includes two convolutional units and a nonlinear mapping unit, comprising one-dimensional dilated causal convolution, weight normalization, ReLU activation function, and Dropout operation.

TCN mainly includes three basic features: causal convolution, dilated convolution, and residual connections. The dilated causal convolution illustrated in Figure 6 is obtained by convolving the input with a causal relationship to generate network output. In sequence modeling, causal convolution means that the current moment T is only related to the inputs at moment T and before. Its mathematical form is described as follows:

Preprints.org (www.preprints.org) | NOT PEER-REVIEWED | Posted: 13 May 2024 doi:10.20944/preprints202405.0814.v1

TCN primarily features three fundamental characteristics: causal convolution, dilated convolution, and residual connections. In sequence modeling, causal convolution ensures that the output at the current time T is only related to inputs at time T and prior times. The mathematical form is described as follows:

$$h_r = f(|x_1|,|x_2|,|\cdots|,|x_T|) \quad (16)$$

where x_T is a one-dimensional vector containing n features, and h_r is the variable to be predicted. f is the function that establishes the relationship between x_T and h_r. Causal convolution is a unidirectional structure, ensuring the sequentiality of data processing by handling the values at moment t and only using data from before moment t For a one-dimensional series input, the dilated convolution operation, $F_{(S)}$ on its elements and the filter f: $\{0, \ldots, k-1\}$ is defined as follows:

$$F_{(S)} = (x * df)(s) = \sum_{i=0}^{k-1} f(i) \bullet x_{s-d \bullet i} | \quad (17)$$

Given s as the input sequence information, d as the dilation factor, and k as the size of the filter, $s - d \bullet i$ represents the location of certain information in the history. As the dilation factor $d = (1,2,4)$ increases, the receptive field of the TCN increases, leading to an increase in the amount of information received. The expanded convolution structure is shown in Figure 7.

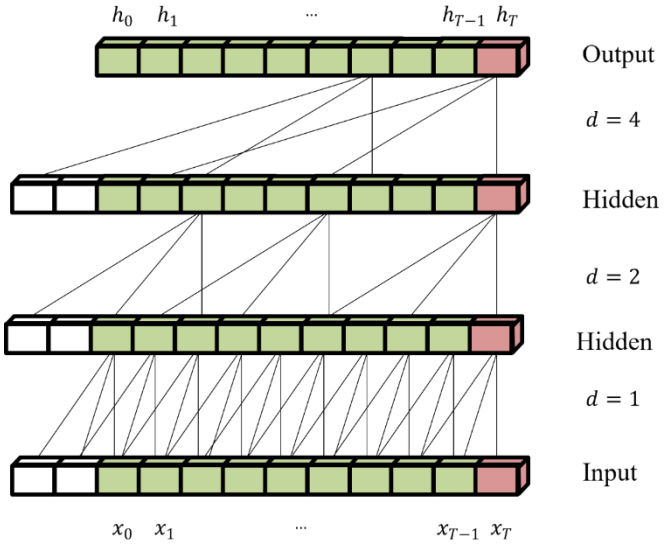

Figure 7. An Expanded Causal Convolution with dilation factors d = 1, 2, 4, and filter size k = 3. (x_T is the input at time step T, h_r is the output vector at time step T).

Residual connections have proven their effectiveness in training deep networks by allowing information to be transmitted across layers. Each residual block includes a branch that leads out a series of transformations F, whose outputs are added to the input X of the block:

$$\beta = Activation(X + F(X)) \quad (18)$$

As shown in Figure 8, within the residual block, the TCN comprises two layers of dilated causal convolutions and nonlinear processing, where Rectified Linear Units (ReLU) are used. For normalization, weight normalization is applied to the convolutional filters. Additionally, after normalization through dilated convolution, a spatial dropout is incorporated in each layer to deactivate some neurons, thus avoiding overfitting.

Preprints.org (www.preprints.org) | NOT PEER-REVIEWED | Posted: 13 May 2024 doi:10.20944/preprints202405.0814.v1

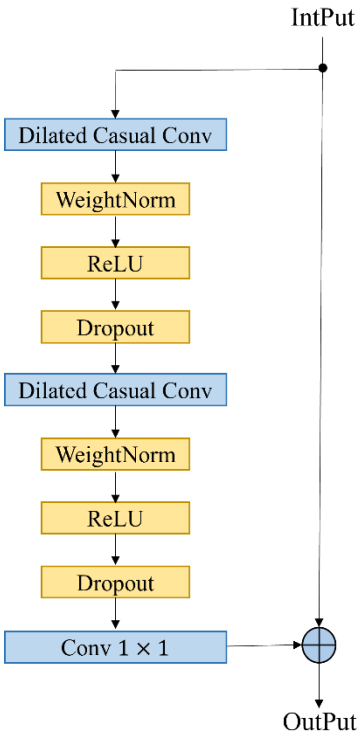

Figure 8. The TCN residual block. (An 1x1 convolution is added when residual input and output have different dimensions.).

2.4.2. LSTM

Long Short-Term Memory neural networks (LSTM) are an optimized variant of Recurrent Neural Networks (RNN), designed to address the issues of vanishing and exploding gradients that are present in traditional neural networks. LSTMs aim to mitigate long-term dependency problems, making them particularly suitable for tasks that require learning from sequences of data over long periods. They have been refined and expanded by numerous scholars in various works and have shown impressive performance across a wide range of time series problems.

An LSTM neural network unit includes three gates: the input gate, output gate, and forget gate. These gates work together to regulate the flow of information into and out of the cell, deciding what to keep in or omit from the cell's state. The architecture of a basic unit and the LSTM network architecture are depicted in the figures (not provided here). As represented in Figure 7 (hypothetically, since the figure is not displayed), the equations for an LSTM unit are as follows:

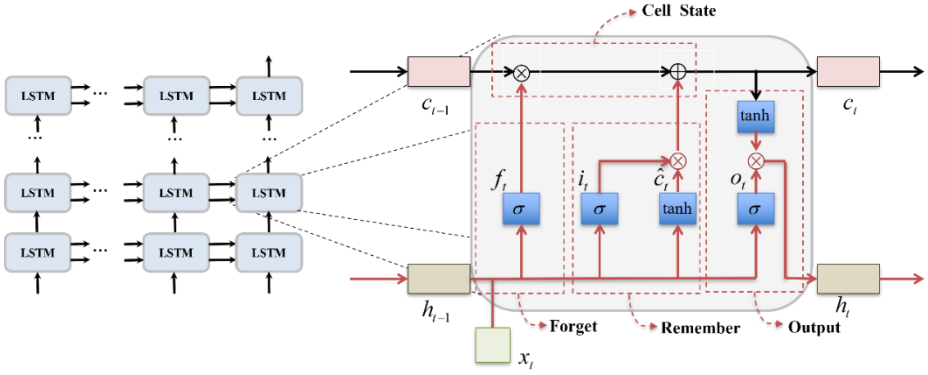

Figure 9. This is a figure. Schemes follow the same formatting.

$$f_t = \sigma(W_f \cdot [h_{t-1}, x_t] + b_f) \quad (19)$$

 doi:10.20944/preprints202405.0814.v1

$$i_t = \sigma(W_i \cdot [h_{t-1}, x_t] + b_i) \quad (20)$$

$$\tilde{C}_t = \tanh(W_C \cdot [h_{t-1}, x_t] + b_C) \quad (21)$$

$$o_t = \sigma(W_o [h_{t-1}, x_t] + b_o) \quad (22)$$

$$h_t = o_t * \tanh(C_t) \quad (23)$$

where W_f, W_i, W_C and W_o represent the weight matrices associated with the forget gate, input gate, candidate values (for updating the cell state), and output gate, respectively. These matrices play crucial roles in determining the flow and transformation of information within the LSTM cell. $h_{t-1}$is the hidden state from the previous time step, carrying information from earlier in the sequence. x_t is the input information at the current time step, introducing new information to be processed. b_f, b_i, b_C and b_o are biases that adjust the output of their respective gates and candidate cell state update mechanisms, adding another level of adaptability to the model. The cell states,C_t and C_{t-1}, represent the memory of the LSTM cell. C_t is the current cell state, and C_{t-1} is the cell state from the previous time step. These states are critical for the LSTM's ability to carry information across long sequences, allowing the network to remember and forget information selectively. $\tilde{C}_t$ represents the candidate cell state, which is a combination of the current input x_t and the previous hidden state h_t. It suggests potential updates to the cell state, providing the model with the option to incorporate new information based on the input and the LSTM's memory. The final decision on which memories to keep or discard—and how much of the new candidate state to add to the existing cell state—is made through the input and forget gates, guided by the LSTM's learned parameters. This architecture enables LSTMs to decide what information is valuable and should be retained over long sequences, making them exceptionally suited for tasks that require understanding and processing sequential data with complex, long-range dependencies.

2.4.3. Attention-Based Tensor Concatenation Module

From Figure 1, it can be seen that the PA-TLA (Parallel Architecture LSTM-TCN-Attention) proposed in this paper is composed of two independent models and a specialized architecture. One is a TCN (Temporal Convolutional Network) with n layers, and the other is an LSTM (Long Short-Term Memory) network with m layers. These two multilayer networks operate independently but share the same input data. Afterward, a tensor fusion module combines the output results of the two networks, The principle is as follows:

$$y_i = RELU(w \sum_{i=1}^{o+\rho} x_i + b) \quad (24)$$

Where y_i represents the target output value, x_i is the input, w denotes the weight values, b stands for the bias values, $RELU$ refers to the Rectified Linear Unit, o is the number of filters in the last stack of the TCN, and ρ is the number of units in the last layer of the LSTM. Due to the lack of sensitivity to the temporal features within the sequence data of LSTM and TCN, they fail to capture the intrinsic connections within the data, limiting their ability to extract and learn important feature information, which is not conducive to further improving the model's prediction accuracy. Therefore, this paper introduces a self-attention mechanism, connecting different positions within the sequence to enhance the model's ability to capture key temporal feature information. First, for each output, the corresponding Query, Key, and Value vectors need to be calculated through three different fully connected layers, as shown in the equation:

$$Q_i = W_Q y_i + b_Q$$

$$K_i = W_K y_i + b_K$$

$$V_i = W_V y_i + b_V \quad (25)$$

 doi:10.20944/preprints202405.0814.v1

Where W_Q, W_K, W_V represent the weight matrix, and b_Q, b_K, b_V are the bias term. Attention scores e_{ij} are computed using the query and key as follows: Where b_{att} is the bias term, W_{att} is the weight matrix, and $\tanh$ represents a nonlinear activation function. Then, the softmax function is applied to normalize the attention scores across all time steps, resulting in the final attention weights a_{ij} as shown in the equation:

$$a_{ij} = \frac{exp(e_{ij})}{\sum_{k=1}^{N} exp(e_{ik})} \quad (26)$$

Finally, the final output is obtained by calculating the weighted sum, as in the equation:

$$z_i = \sum_{j=1}^{N} a_{ij} V_j \quad (27)$$

3. Experiments

3.1. Material Preparation

3.1.1. Wake Vortex CFD Numerical Simulation Data

In experiments involving numerical simulation of aircraft wake vortex dissipation, data on the evolution of vortices from an A330-200 aircraft within a height range of 5-300m above ground level (with 1m intervals) was collected. This included aircraft and environmental parameters, which are detailed in Table 1. Through these complex numerical simulations, a total data volume of approximately 14.3TB was generated, detailing the evolution of the wake vortex.

Table 1. Relevant parameters of the Airbus A330-200 model.

Environmental Parameter	
Ambient Temperature	20℃
Atmospheric Pressure	1atm
Air Density	1.225kg/m³
Aircraft Parameters	
Wingspan	60.3m
Maximum Landing Weight	182000kg
Speed	72m/s
Initial Vortex Circulation	427m²/s
Vortex Core Radius	3m≈0.052B
Initial Vortex Spacing	47.36m≈B*Pi/4
Characteristic Speed	1.436m/s
Characteristic Duration	33s

The vortex core radius (r_c) is the radial distance from the center of the vortex core to the point in the nearby flow field where the tangential velocity reaches its maximum value. It is an important parameter for measuring the distribution of aircraft wake vortices. In numerical simulation studies of wake vortices, the selected values for the vortex core radius vary among different references. For ideal aircraft wake vortices, the range of values for the vortex core radius generally lies between $r_c / b_0 = 1\% - 7\%$. This paper references the value for r_c / b_0 used by Holzäpfel [4] in their research, which is 5.2%.

Preprints.org (www.preprints.org) | NOT PEER-REVIEWED | Posted: 13 May 2024 doi:10.20944/preprints202405.0814.v1

Figure 10 shows the variation of wake vortex vorticity and tangential velocity over time under calm wind conditions. Analysis reveals that, in the initial stage after detachment, the wake vortex has a relatively small impact range, forming a sudden change area of vorticity only near the vortex core, with a vorticity extreme point appearing at the center of the vortex core, approximately 12s $^{-1}$. Outside the vortex core area, as the radial distance from the vortex center increases, the vorticity gradually decreases. Subsequently, influenced by gravity and the mutual induction between wake vortices, the wake vortex gradually shows a downward trend, and the affected area of the wake vortex begins to expand. By 33 seconds, under calm wind conditions, the vorticity cloud map of the wake vortex shows that the impact range of the wake vortex has significantly expanded compared to the initial stage, but the maximum vorticity value at the vortex core has significantly decreased. Around 66 seconds, the interaction effect between wake vortices gradually strengthens, and a merging trend appears in the flow field surrounding the wake vortices.

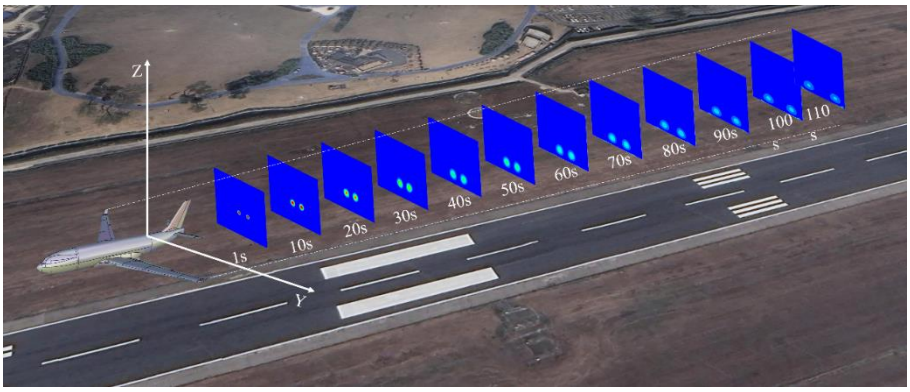

Figure 10. Aircraft Wake Vortex Vorticity Cloud Diagram at Decision Height under Calm Wind Conditions.

3.1.2. CFD Data Validation

Using lidar data to validate CFD data ensures that the model can accurately predict the behavior of wake vortices. The study employed the Wind3D 6000 aviation meteorological lidar developed jointly by Ocean University of China and Qingdao Ray Measurement and Control Technology Co., Ltd. This device can continuously measure three-dimensional vertical wind profiles, wind speed, and wind direction, obtaining high-precision real-time wind field data.

Filter the evolution data of the wake vortex for the A330 model at wind speeds close to calm, and compare the numerically simulated wake vortex radial velocity with the laser radar detected wake vortex radial velocity. As shown in Figure 11, it displays two sets of velocity pairs in opposite directions, and the distribution of the velocity pairs satisfies rotational symmetry.

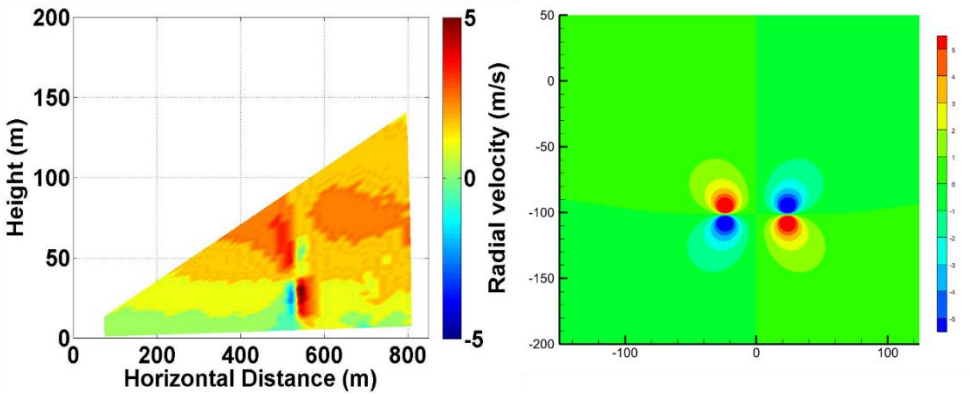

Figure 11. Comparison of CFD numerical simulation data and LiDAR wake detection data.

 doi:10.20944/preprints202405.0814.v1

We extracted the circulation characteristics of aircraft wake from LIDAR data and compared them with the circulation characteristics derived from CFD data at corresponding altitudes, as shown in Figure 12. The results indicate that the CFD evolution data obtained experimentally aligns closely with the evolution patterns of aircraft wakes derived from field-detected LIDAR data.

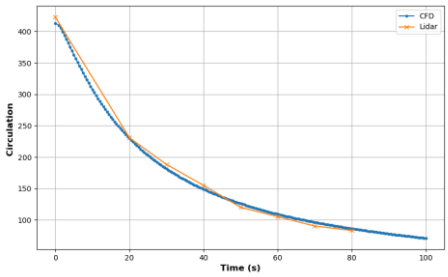

Figure 12. Comparison of circulation characteristic parameters between LIDAR data and CFD data.

3.2. Evaluation Criteria

In this study, we use normalized Mean Absolute Error (MAE), normalized Mean Squared Error (MSE), normalized Root Mean Squared Error (RMSE), and R^2 as evaluation metrics to assess the predictive performance of the model. Furthermore, MSE is used as a measure of accuracy during model training.

$$MAE = \frac{1}{n}\sum_{i=1}^{n}| y_i - \hat{y}_i | \quad (28)$$

$$RMSE = \sqrt{\frac{1}{n}\sum_{i=1}^{n}(y_i - \hat{y}_i)^2} \quad (29)$$

$$\mathrm{MSE} = \frac{1}{n}\sum_{i=1}^{n}(y_i - \hat{y}_i)^2. \quad (30)$$

$$R^2 = 1 - \frac{\Sigma_{i=1}^{n}(y_i - \hat{y}_i)^2}{\Sigma_{i=1}^{n}(y_i - \bar{y}_i)^2} \quad (31)$$

Where: γ_i *is the predicted value;* $\hat{y}_i$ *is the actual value; n is the number of samples*

3.3. PA-TLA Parameter Configuration

PA-TLA is a parallel architecture composed of two layers of convolutionally stacked TCN (Temporal Convolutional Networks) and three layers of LSTM (Long Short-Term Memory). We set the time step to 12, use the Adam optimizer during training, employ MSE (Mean Squared Error) as the loss function, maintain a batch size of 64, and run the model for 150 epochs. As depicted in Figure 13, the loss on the training and validation datasets evolves throughout the training epochs. Clearly, after all iterations, the model exhibits no signs of overfitting.

Preprints.org (www.preprints.org) | NOT PEER-REVIEWED | Posted: 13 May 2024 doi:10.20944/preprints202405.0814.v1

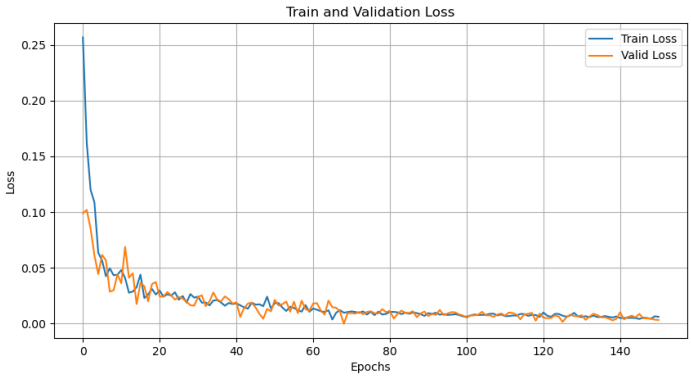

Figure 13. The loss changes of PA-TLA on the training set and validation.

3.4. Results Analysis

3.4.1. Wake Evolution Prediction Model Based on PA-TLA

To further demonstrate the effectiveness of PA-TLA, we constructed a TCN-LSTM structure composed of a two-layer convolutional stacked TCN and a three-layer LSTM in series. As illustrated in Figure 14a–f. This figure shows the comparison of predicted and actual vorticity characteristic parameters for four models: PA-TLA, TCN-LSTM, LSTM, and TCN, all of which exhibit high levels of fit

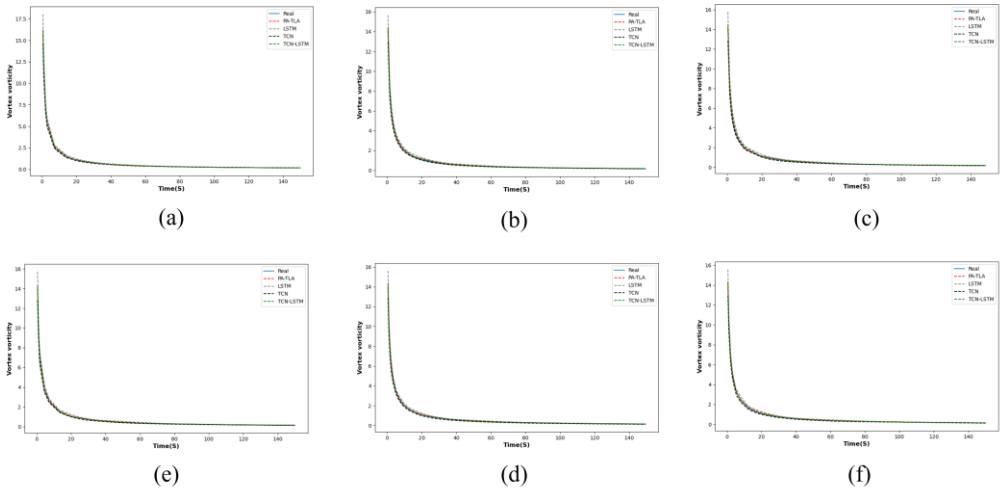

Figure 14. Comparison of the Predictive Performance of Three Models on Aircraft Wake Vorticity(A for 50 meters, B for 100 meters, C for 150 meters, D for 200 meters, E for 250 meters, F for 300 meters);.

To further observe the prediction errors of the four models, Figure 14 presents the relative error plots for the predicted vorticity characteristic parameters. It is evident that TCN, with its capability to perceive spatial features of the sequence, performs better in terms of relative error compared to LSTM. Both PA-TLA and TCN-LSTM, which integrate the spatial feature perception of TCN with the temporal feature perception of LSTM, show good performance in predicting aircraft wake characteristic parameters, with PA-TLA outperforming TCN-LSTM in relative error.

Preprints.org (www.preprints.org) | NOT PEER-REVIEWED | Posted: 13 May 2024 doi:10.20944/preprints202405.0814.v1

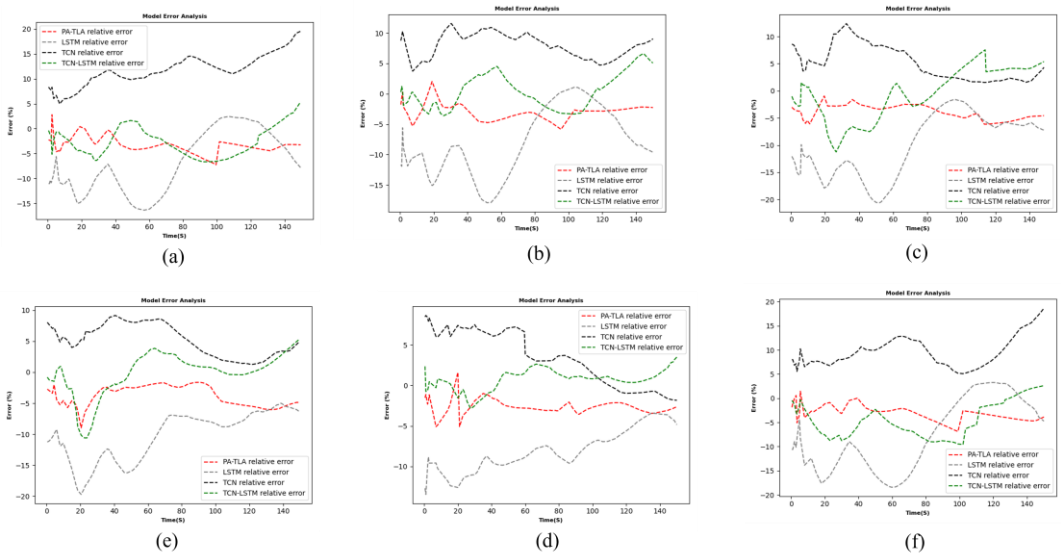

Figure 15. Relative Error in Q-Criterion Prediction for Three Models (A for 50 meters, B for 100 meters, C for 150 meters, D for 200 meters, E for 250 meters, F for 300 meters).

Table 2 reveals that across different heights, the models predict wake circulation, vorticity, and Q-criterion. PA-TLA and TCN-LSTM outperform LSTM and TCN on all error metrics, exhibiting lower mean squared error (MSE), mean absolute error (MAE), root mean square error (RMSE), and higher coefficient of determination (R^2), indicating superior model fit and significantly enhanced predictive accuracy on this dataset. Moreover, compared to TCN-LSTM, PA-TLA shows an average reduction in MSE by 6.80%, in MAE by 7.70%, in RMSE by 4.47%, and an average increase in R^2 by 0.36%. The training time for the PA-TLA model is approximately 144 minutes, and prediction time is about 292 seconds, whereas the TCN-LSTM requires 201 minutes for training and 380 seconds for prediction, demonstrating a 28% improvement in training efficiency and a 35% increase in prediction efficiency for the parallel structure over the serial model structure.

Table 2. The prediction results of the three models on the testing set.

Feature	Model	MSE	MAE	RMSE	R^2
Q Criterion	TCN	0.239	0.086	0.149	97.891
	LSTM	0.274	0.091	0.189	97.147
	TCN-LSTM	0.205	0.073	0.134	98.712
	PA-TLA	0.191	0.066	0.129	99.161
Vorticity	TCN	0.109	0.123	0.331	97.163
	LSTM	0.113	0.136	0.335	96.934
	TCN-LSTM	0.085	0.096	0.267	97.934
	PA-TLA	0.079	0.088	0.252	98.256
Circulation	TCN	12.749	2.968	4.192	96.736
	LSTM	13.141	3.352	4.753	96.356
	TCN-LSTM	10.356	2.105	3.206	97.846
	PA-TLA	9.682	1.956	3.075	98.158

 doi:10.20944/preprints202405.0814.v1

3.4.2. Analys3.4.2. Analysis of Near-Ground Phase Wake Vortex Evolution Characteristics Combining Numerical Simulation and PA-TLA Model

The experiment, focusing on the A330-200 model, predicts different stages of wake evolution in the near-ground phase through the proposed PA-TLA model, selecting circulation and vortex core position as parameters for quantitative analysis of vortex characteristics. Figure 1a shows that at different height conditions, the model-predicted average vortex circulation follows a negative exponential decay rule through the initial stage, rapid decay, and gradual transition to a stable evolution pattern. Within 0-10s, the vortex structure remains tight and concentrated, with circulation concentrated near the vortex core. For lower altitude vortices, the distance between the vortex and the ground is smaller, which might lead to stronger constraints and deformation of the vortex structure, differing in the specific form of initial circulation distribution. During the rapid decay phase of 10-20s, air viscosity causes circulation within the vortex to diffuse and dissipate radially and axially through friction and mixing processes within micro-scale vortices, accelerating the reduction of circulation. Moreover, for low altitude vortices, the shear layer thickness between them and the ground is thinner, making the viscous effects more significant and further intensifying the dissipation of circulation. However, after 80s, as the vortex structure gradually diffuses, part of the circulation may reorganize into secondary vortices or vortex filaments, forming more complex vortex structures. Despite the potential continued decrease in circulation, the change in vortex morphology can slow its further decay. From 10m-50m, as the height increases, the effect of ground influence weakens, increasing the rate of wake decay. From 50m-300m, the rate of wake decay is almost consistent.

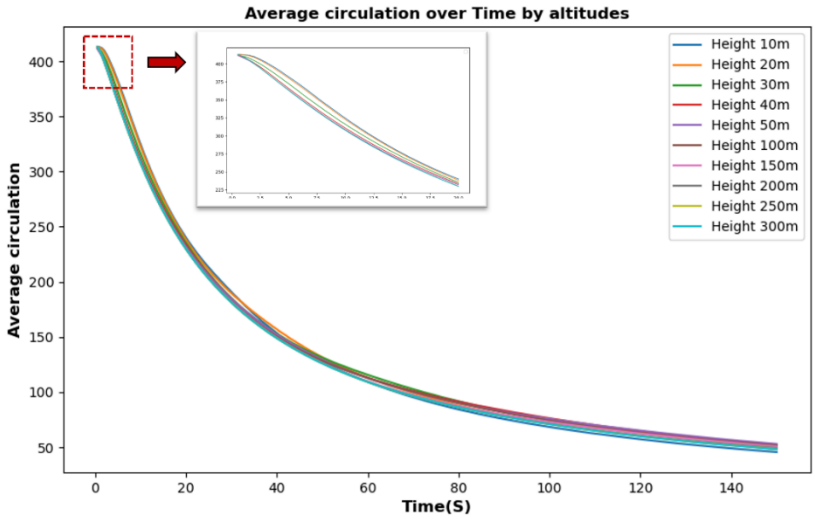

Figure 18. Evolution Curve of Aircraft Wake Circulation at Different Heights.

The time-dependent evolution trend of vortex core position at different initial heights is shown in figures (a) and (b). The vortex core height curves show a consistent time-decreasing characteristic at different initial heights, exhibiting a sharp decline rate in line with theory due to increased viscous resistance intensifying local dissipation of vorticity in the early phase (approximately the first 25 seconds). However, as time progresses, the influence domain of the tail vortex expands, the velocity difference between the vortex core and the surrounding flow field decreases, and the induced effect and air resistance cause the interaction between vortices to weaken, leading to a gradually stabilizing vortex core sinking speed. Near the ground, the lateral spacing evolution trend of the wake vortex, as shown in figure (c), exhibits a non-linear expansion characteristic over time. The presence of the ground not only changes the flow state of the boundary layer but also enhances vortex diffusion in the near-ground region, promoting a faster growth rate of vortex spacing. Moreover, from 10m-50m, affected by ground effect, the higher the altitude, the faster the decay rate, and the vortex core position initially sinks briefly before showing an upward trend, while the ground effect induces an increase

 doi:10.20944/preprints202405.0814.v1

in the distance between two vortices, developing towards isolated vortex stages and weakening the mutual induction forces between them.

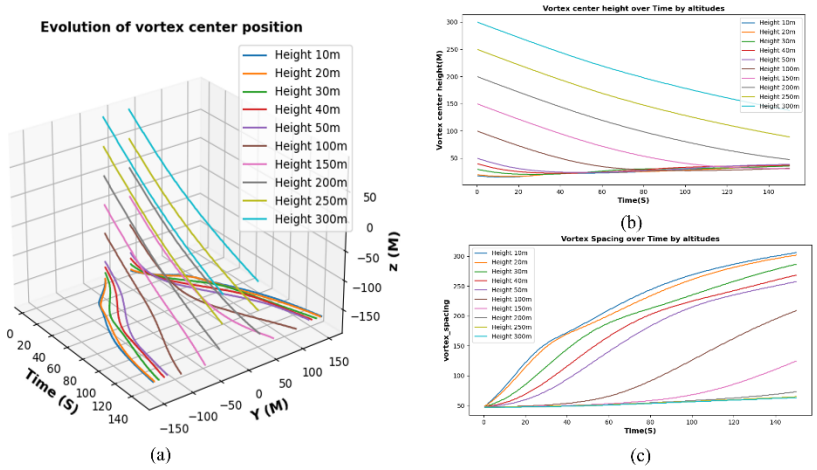

Figure 19. Evolution of Vortex Core Position of Aircraft Wake at Different Heights((a) represents the three-dimensional variation curve of the vortex center of the aircraft wake, (b) represents the evolution of the longitudinal position of the vortex center, and (c) represents the evolution of the distance between the two vortex centers).

Conclusion

This study uses CFD numerical simulation data and constructs a PA-TLA model based on a hybrid parallel architecture for predicting the evolution of wake vortex characteristic parameters at different initial heights during the approach phase. The results are as follows:

(1). Using PA-TLA to predict the circulation, Q criterion, and vorticity of wake vortices at different initial heights outperforms both the LSTM and TCN in various predictive indicators. Compared to traditional CFD methods, this model improves computational efficiency by approximately 40 times.

(2). Different initial heights have a certain impact on the evolution of wake vortices. The circulation of aircraft wake vortices continuously decays, and at heights of 10m-50m, affected by ground effect, the higher the altitude, the faster the decay rate. Additionally, the vortex core position initially sinks briefly before showing an upward trend. The ground effect induces an increase in the distance between two vortices, developing towards isolated vortex stages and weakening the mutual induction forces between them. From 50m-300m, as the ground effect weakens, the circulation declines in almost the same trend, and the vortex core position continues to drop.

(3). This study provides important insights for the research of paired approach wake separation. The proposed model effectively reduces the computational time for aircraft wake evolution characteristics. This research enables a more detailed exploration of safe wake intervals for paired aircraft at different altitudes. Our study only considered the characteristics of aircraft wake evolution during the approach phase under calm wind conditions and constructed a preliminary data prediction using PA-TLA. In the future, more scenarios will be added, such as different aircraft types, side winds, headwinds, temperature, humidity conditions for aircraft wake evolution characteristics, and calculating the safe wake intervals for different aircraft combinations, establishing a wake evolution characteristic database for rapid prediction of wake safe intervals.

Author Contributions: Conceptualization, L.D. and W.P.; methodology, L.D.; software, L.D.; validation, L.D., Y.L. and T.L.; formal analysis, L.D.; investigation, L.D.; resources, L.D.; data curation, T.L and L.D.; writing—original draft preparation, L.D.; writing—review and editing, L.D.; visualization, W.P. amd L.D.; supervision, L.D.; project administration, W.P.; funding acquisition, W.P. All authors have read and agreed to the published version of the manuscript.

Funding: This research was funded by the National Key R&D Program of China (No. 2021YFF0603904), National Natural Science Foundation of China (U1733203), (U2333209) Civil Aviation Administration Safety Capacity Building Project TM2019-16-1/3, the Civil Aviation Administration of China (AQ20200019), and Student Innovation Fund Program (24CAFUC10182), (S202310624091).

Data Availability Statement: The authors confirm that the data supporting the findings of this study are available within the article.

Conflicts of Interest: The authors declare no conflicts of interest.

References

1. Lauer, N.; Yeo, D.W.; Snyder, D.A.; Paley, D.A. Tip-Vortex Localization for Cross-Stream Position Control of a Multi-Hole Probe Relative to a Stationary Wing in a Free-Jet Wind Tunnel. In Proceedings of the AIAA Guidance, Navigation, and Control Conference; American Institute of Aeronautics and Astronautics: Reston, Virginia, January 5 2017.
2. Gerz, T.; Holzäpfel, F.; Darracq, D. Commercial Aircraft Wake Vortices. Progress in Aerospace Sciences 2002, 38, 181–208, doi:10.1016/s0376-0421(02)00004-0.
3. De Visscher, I.; Bricteux, L.; Winckelmans, G. Aircraft Vortices in Stably Stratified and Weakly Turbulent Atmospheres: Simulation and Modeling. AIAA Journal 2013, 51, 551–566, doi:10.2514/1.j051742.
4. Tang, Z.-G., Zhu, L.-Y.; Xiang, X.-H; et al. Several research progress and prospects of intelligent aerodynamics. Chinese Journal of Aerodynamics,2023,41, 1-35.
5. Zheng, T.-Y.; Wang, S.-Y.; Wang, G.-X.; Deng, X.-G. High-Order Natural Transition Simulation Method Based on Deep Residual Network. Acta Physica Sinica 2020, 69, 204701, doi:10.7498/aps.69.20200563.
6. Wu, L.; Cui, B.; Xiao, Z. Artificial Neural Network-Based One-Equation Model for Simulation of Laminar-Turbulent Transitional Flow. Theoretical and Applied Mechanics Letters 2023, 13, 100387, doi:10.1016/j.taml.2022.100387.
7. Carpenter, M.; Hartfield, R.; Burkhalter, J. A Comprehensive Approach to Cataloging Missile Aerodynamic Performance Using Surrogate Modeling Techniques and Statistical Learning. In Proceedings of the 29th AIAA Applied Aerodynamics Conference; American Institute of Aeronautics and Astronautics: Reston, Virigina, June 27 2011.
8. Balla, K.; Sevilla, R.; Hassan, O.; Morgan, K. An Application of Neural Networks to the Prediction of Aerodynamic Coefficients of Aerofoils and Wings. Applied Mathematical Modelling 2021, 96, 456–479, doi:10.1016/j.apm.2021.03.019.
9. Wang, Z.; Xiao, D.; Fang, F.; Govindan, R.; Pain, C.C.; Guo, Y. Model Identification of Reduced Order Fluid Dynamics Systems Using Deep Learning. International Journal for Numerical Methods in Fluids 2017, 86, 255–268, doi:10.1002/fld.4416.
10. Luo, H.; Pan, W.; Wang, Y.; Luo, Y. A330-300 Wake Encounter by ARJ21 Aircraft. Aerospace 2024, 11, 144, doi:10.3390/aerospace11020144.
11. Xu, Y.; Sha, Y.; Wang, C.; Cao, W.; Wei, Y. Comparative Studies of Predictive Models for Unsteady Flow Fields Based on Deep Learning and Proper Orthogonal Decomposition. Ocean Engineering 2023, 272, 113935, doi:10.1016/j.oceaneng.2023.113935.
12. He, X.; Zhao, R.; Gao, H.; Yuan, C.; Wang, J. Prediction of Aircraft Wake Vortices under Various Crosswind Velocities Based on Convolutional Neural Networks. Sustainability 2023, 15, 13383, doi:10.3390/su151813383.
13. Rojas, J.I.; Melgosa, M.; Prats, X. Sensitivity Analysis of Maximum Circulation of Wake Vortex Encountered by En-Route Aircraft. Aerospace 2021, 8, 194, doi:10.3390/aerospace8070194.
14. Holzäpfel, F.; Steen, M. Aircraft Wake-Vortex Evolution in Ground Proximity: Analysis and Parameterization. In Proceedings of the 44th AIAA Aerospace Sciences Meeting and Exhibit; American Institute of Aeronautics and Astronautics: Reston, Virigina, January 9 2006.
15. Holzäpfel, F. Probabilistic Two-Phase Wake Vortex Decay and Transport Model. Journal of Aircraft 2003, 40, 323–331, doi:10.2514/2.3096.
16. Sekine, K.; Kato, F.; Kageyama, K.; Itoh, E. Data-Driven Simulation for Evaluating the Impact of Lower Arrival Aircraft Separation on Available Airspace and Runway Capacity at Tokyo International Airport. Aerospace 2021, 8, 165, doi:10.3390/aerospace8060165.
17. Gerz, T.; Holzäpfel, F.; Darracq, D. Commercial Aircraft Wake Vortices. Progress in Aerospace Sciences 2002, 38, 181–208, doi:10.1016/s0376-0421(02)00004-0.
18. Crow, S. Stability Theory for a Pair of Trailing Vortices. In Proceedings of the 8th Aerospace Sciences Meeting; American Institute of Aeronautics and Astronautics: Reston, Virigina, January 19 1970.
19. Holzäpfel, F.; Hofbauer, T.; Darracq, D.; Moet, H.; Garnier, F.; Gago, C.F. Analysis of Wake Vortex Decay Mechanisms in the Atmosphere. Aerospace Science and Technology 2003, 7, 263–275, doi:10.1016/s1270-9638(03)00026-9.

20. Han, J.; Lin, Y.-L.; Arya, S.; Proctor, F. Large Eddy Simulation of Aircraft Wake Vortices in a Homogeneous Atmospheric Turbulence - Vortex Decay and Descent. In Proceedings of the 37th Aerospace Sciences Meeting and Exhibit; American Institute of Aeronautics and Astronautics: Reston, Virigina, January 11 1999.
21. Holzäpfel, F.; Gerz, T.; Baumann, R. The Turbulent Decay of Trailing Vortex Pairs in Stably Stratified Environments. Aerospace Science and Technology 2001, 5, 95–108, doi:10.1016/s1270-9638(00)01090-7.
22. 2017, 30, 1866–1876, doi:10.1016/j.cja.2017.08.012.
23. Harvey, J.K.; Perry, F.J. Flowfield Produced by Trailing Vortices in the Vicinity of the Ground. AIAA Journal 1971, 9, 1659–1660, doi:10.2514/3.6415.
24. Harris, D.M.; Williamson, C.H.K. Instability of Secondary Vortices Generated by a Vortex Pair in Ground Effect. Journal of Fluid Mechanics 2012, 700, 148–186, doi:10.1017/jfm.2012.108.
25. Breitsamter, C. Wake Vortex Characteristics of Transport Aircraft. Progress in Aerospace Sciences 2011, 47, 89–134, doi:10.1016/j.paerosci.2010.09.002.
26. Holzäpfel, F.; Gerz, T.; Köpp, F.; Stumpf, E.; Harris, M.; Young, R.I.; Dolfi-Bouteyre, A. Strategies for Circulation Evaluation of Aircraft Wake Vortices Measured by Lidar. Journal of Atmospheric and Oceanic Technology 2003, 20, 1183–1195, doi:10.1175/1520-0426(2003)020<1183:sfceoa>2.0.co;2.
27. Rojas, J.I.; Melgosa, M.; Prats, X. Sensitivity Analysis of Maximum Circulation of Wake Vortex Encountered by En-Route Aircraft. Aerospace 2021, 8, 194, doi:10.3390/aerospace8070194.
28. Hirsch, C. Numerical Simulation of Inviscid Flows. In Numerical Computation of Internal and External Flows; Elsevier, 2007; pp. 545–597.
29. Luo, H.; Pan, W.; Wang, Y.; Luo, Y. A330-300 Wake Encounter by ARJ21 Aircraft. Aerospace 2024, 11, 144, doi:10.3390/aerospace11020144.